Journal of Hazardous Materials 219–220 (2012) 13–18

Contents lists available at SciVerse ScienceDirect

Journal of Hazardous Materials

journal homepage: www.elsevier.com/locate/jhazmat

Synthesis of TiO_2 nanorod-decorated graphene sheets and their highly efficient photocatalytic activities under visible-light irradiation

Eunwoo Lee, Jin-Yong Hong, Haeyoung Kang, Jyongsik Jang*

World Class University (WCU) Program of Chemical Convergence for Energy & Environment (C_2E_2), School of Chemical and Biological Engineering, College of Engineering, Seoul National University (SNU), 599 Gwanangno, Gwanak-gu, Seoul 151-742, Republic of Korea

ARTICLE INFO

Article history:
Received 29 August 2011
Received in revised form
30 November 2011
Accepted 10 December 2011
Available online 19 December 2011

Keywords:
TiO_2
Graphene
Photocatalysis
Photoelectrochemistry
Methylene blue

ABSTRACT

The titanium dioxide (TiO_2) nanorod-decorated graphene sheets photocatalysts with different TiO_2 nanorods population have been synthesized by a simple non-hydrolytic sol–gel approach. Electron microscopy and X-ray diffraction analysis indicated that the TiO_2 nanorods are well-dispersed and successfully anchored on the graphene sheet surface through the formation of covalent bonds between Ti and C atoms. The photocatalytic activities are evaluated in terms of the efficiencies of photodecomposition and adsorption of methylene blue (MB) in aqueous solution under visible-light irradiation. The as-synthesized TiO_2 nanorod-decorated graphene sheets showed unprecedented photodecomposition efficiency compared to the pristine TiO_2 nanorods and the commercial TiO_2 (P-25, Degussa) under visible-light. It is believed that this predominant photocatalytic activity is due to the synergistic contribution of both a retarded charge recombination rate caused by a high electronic mobility of graphene and an increased surface area originated from nanometer-sized TiO_2 nanorods. Furthermore, photoelectrochemical study is performed to give deep insights into the primary roles of graphene that determines the photocatalytic activity.

1. Introduction

Photocatalyst, which accelerates light-driven chemical reactions, has been paid a great attention due to fascinating properties such as quantum confinement and enhanced reactivity. The photocatalytic materials could be applied for the potential fields including self-cleaning surface, water splitting, and air/water purification. The most important application field in photocatalysts is in the purification field, such as degradation of organic pollutants in water at ambient conditions with the use of inexpensive and clean solar light and atmospheric dioxygen as the energy source and oxidant, respectively.

Up to date, diverse photocatalytic materials have been introduced, including TiO_2, ZnO, CdS, Fe_3O_4, SnO_2, V_2O_3, and WO_3 [1–5]. Among them, TiO_2 and its derivatives have stimulated a great deal of interest because of their advantages, which include low cost, reliability, strong oxidization power, environmental nontoxicity, high stability, and chemical/biological inertness [6–9].

Graphene, an atomic sheet of sp^2-bonded carbon atoms arranged in a honeycomb structure [10,11], as recently been highlighted as a promising composite material with TiO_2 due to the following advantages. First, the retarded charge recombination is useful because the high electronic conductivity of graphene leads to facile charge transportation and separation. Second, it has increased reaction sites because the high surface to volume ratio with the two-dimensional planner structure of graphene creates a large specific surface area. The third advantage is an expanded light absorption range because the facile control of the energy bandage modified by carbon-doping enhances broad light absorption. Finally, these composites have an enhanced dye-quenching efficiency because the strong interaction from the π–π stacking between aromatic regions of graphene and pollutant molecules leads to high affinity and fast adsorptivity. Nevertheless, few reports have focused on the preparation of TiO_2/graphene composite materials for visible light-driven photocatalytic applications due to the difficulty of TiO_2 treatments [12,13]. However, most of the previous researches were conducted using lengthy experimental anchoring steps as well as with TiO_2 nanocrystals anchored on a limited region of graphene layers [14–16]. Therefore, it is imperative to develop the simple and reliable methodology for TiO_2/graphene nanocomposite photocatalyst.

Herein, we present the simple synthetic route for the fabrication of TiO_2 nanorod-decorated graphene sheets (TNGSs) via a non-hydrolytic sol–gel reaction. The population of TiO_2 nanorods can be controlled easily by changing the concentration of GO (wt%), and the photocatalytic activities are evaluated in terms of the

* Corresponding author. Tel.: +82 2 880 7069; fax: +82 2 888 1604.
E-mail address: jsjang@plaza.snu.ac.kr (J. Jang).

0304-3894/$ – see front matter © 2011 Elsevier B.V. All rights reserved.
doi:10.1016/j.jhazmat.2011.12.033

efficiencies of photodecomposition and adsorption of methylene blue (MB) in aqueous solution under visible-light irradiation. Furthermore, photoelectrochemical study is performed to give deep insights into the primary roles of graphene sheets that determine the photocatalytic activity.

2. Experimental

2.1. Materials.

Graphite powder, titanium (IV) chloride, oleylamine (70%) and toluene (99.5%) were purchased from Aldrich Chemical Co. Commercial TiO_2 (P25) was purchased from Degussa. Methylene blue (MB) was obtained commercially from Aldrich Chemical Co. Unless otherwise specified, other reagents and materials involved were obtained commercially from Aldrich Chemical Co. And used as received without further purification.

2.2. Preparation of graphene oxide (GO)

The graphite oxide was synthesized from natural graphite powder based on Hummers method [17]. In detail, 1 g of graphite was put into a mixture of 1.5 mL of concentrated H_2SO_4, 0.5 g of $K_2S_2O_8$, and 0.5 g of P_2O_5. The solution was heated to 80 °C and kept stirring for 5 h. Then the mixture was diluted with 500 mL of deionized water and the product was obtained by filtering water until the solution is completely neutralized. Finally, the product was dried in air at overnight.

2.3. Synthesis of TiO_2 nanorods decorated graphene sheets (TNGSs)

TNGSs were fabricated via a non-hydrolytic sol–gel reaction [18]. A variable amount of GO was dispersed in 30.5 mL of oleylamine solution. The weight concentration of GO varied in the range of 1–10 wt%. For a complete exfoliation of GO, the mixture was ultrasonicated for 3 h. Next, the exfoliated GO solution was transferred into a three-neck round-bottom flask and heated to 290 °C with nitrogen purging. $TiCl_4$ (0.5 mL) was then injected into the solution under vigorous stirring. The color of the solution changed from dark purple to yellow during the reaction, indicating that TiO_2 nanorods were formed by the non-hydrolytic sol–gel reaction. After 15 min, the reaction was quenched by the addition of 6 mL toluene and then the reaction mixture was allowed to cool to room temperature. The resultant product was separated from the surfactants by centrifugation using an excess of acetone. The products were ultimately retrieved and allowed to dry in a vacuum oven for 12 h. Finally, the products were calcinated for 2 h at 500 °C under a N_2 atmosphere to achieve high crystallinity [19].

2.4. Characterization of the TiO_2 nanorods decorated graphene sheets

The TEM images were taken with a JEOL EM-2000 EX II microscope. To observe TEM images, the TNGSs diluted in toluene were deposited on a carbon film coated copper grid. TNGSs were characterized by high-powder X-ray diffraction (XRD, M18XHF-SRA (Mac Science Co.)) with a Cu Kα radiation source (λ = 1.5406 Å) at 40 kV and 300 mA (12 kW), and field emission scanning electron microscopy (FE-SEM, JEOL-6700) equipped with energy dispersive X-ray spectroscopy (EDS). The spectra of X-ray photoelectron spectroscopy (XPS) were obtained by Sigma probe (Thermo). Lamda 35 (Perkin–Elmer) provided the spectra of UV–vis spectroscopy.

2.5. Photocatalytic activity

Photocatalytic activities of TNGSs were measured by the photodecomposition of methylene blue with concentration at 30 μM. As a controlled sample, Degussa P25 was prepared. For the photodecomposition, 0.030 g of photocatalyst was suspended in a 40 mL of methylene blue aqueous solution and the solution was stirred in a dark room for 2 h to complete the absorption equilibrium. Visible light irradiation to the solution was performed Osram XBO 150-W xenon arc lamp installed in a light-condensing lamp housing (PTI, A1010S). A 455 nm cut-off filter was used and the temperature of the solution was maintained at room temperature by water jacket during the overall degradation process. Moreover, UV light irradiation to the solution was performed by a mercury lamp (300 W), characterized by a main emission peak of 365 nm.

2.6. Photoelectrochemistry

Photoelectrochemical characterization was carried out using a standard three compartment cell, consisting of a working electrode, a platinum wire (counter electrode) and an Ag/AgCl electrode (reference electrode). The as-synthesized TNGSs were mixed with 15 wt% acetylene black (AB) as an electron conductor and 10 wt% poly(vinylidene fluoride) (PVDF) solution dissolved in N-methyl-2-pyrrolidone (NMP) as a binder. The TNGSs electrodes were made by dispersing 90 wt% active materials and 10 wt% PVDF binder in NMP solvent. The resultant slurries were spread on a copper mesh, dried at 110 °C under vacuum overnight to remove the NMP, and then pressed into a sheet. The electrolyte was 0.1 M tetrabutylammonium tetrafluoroborate (NBu_4BF_4) in acetonitrile (AN). The illumination source was a 300 W mercury lamp, characterized by an emission peak of 365 nm. A Keithley 2400 SourceMeter and a Wonatech WBCS 3000 potentiostat were employed for recording the *I–V* and amperometric characteristics.

3. Results and discussion

3.1. Fabrication of TNGSs

To determine the morphology, crystallite size and composition of the as-synthesized TNGSs, the TEM, SEM, mapping, and EDS were analyzed in Fig. 1. The TEM observation revealed that the TiO_2 nanorods exhibited dimensions of 25 nm (length) × 4 nm (diameter) (L/D ratio ≈ 6).

Importantly, these TiO_2 nanorods (NRs) showed a considerably uniform dispersion on the graphene sheets surface. The EDS mapping images of TNGSs also showed Ti and C atoms are well-dispersed.

The EDS analysis indicated the presence of C (5.57%), O (49.81%), and Ti (44.62%), which presented that TiO_2 NRs were uniformly dispersed on the carbonaceous graphene sheets. The surface decorated TiO_2 NRs result in a relatively lower intensity of carbon content compared to higher intensity of titanium content.

The TNGSs were further characterized by XRD and UV–vis absorption spectrum as shown in Fig. 2. In the XRD spectrum of pristine TiO_2 NRs and TNGSs, the diffraction patterns show a large peak centered at $2\theta = 26.5^\circ$, which corresponds to the anatase (1 0 1) interlayer spacing of 3.5 Å. As a result, the XRD patterns of TiO_2 NRs and TNGSs clearly confirmed crystalline anatase TiO_2. The UV–vis absorption spectra of TiO_2 NRs and TNGSs are shown in Fig. 2b. A redshift of about 20 nm was observed in the absorption edge of the TNGSs compared to that of pristine TiO_2 NRs, which was attributable to the narrowing of the

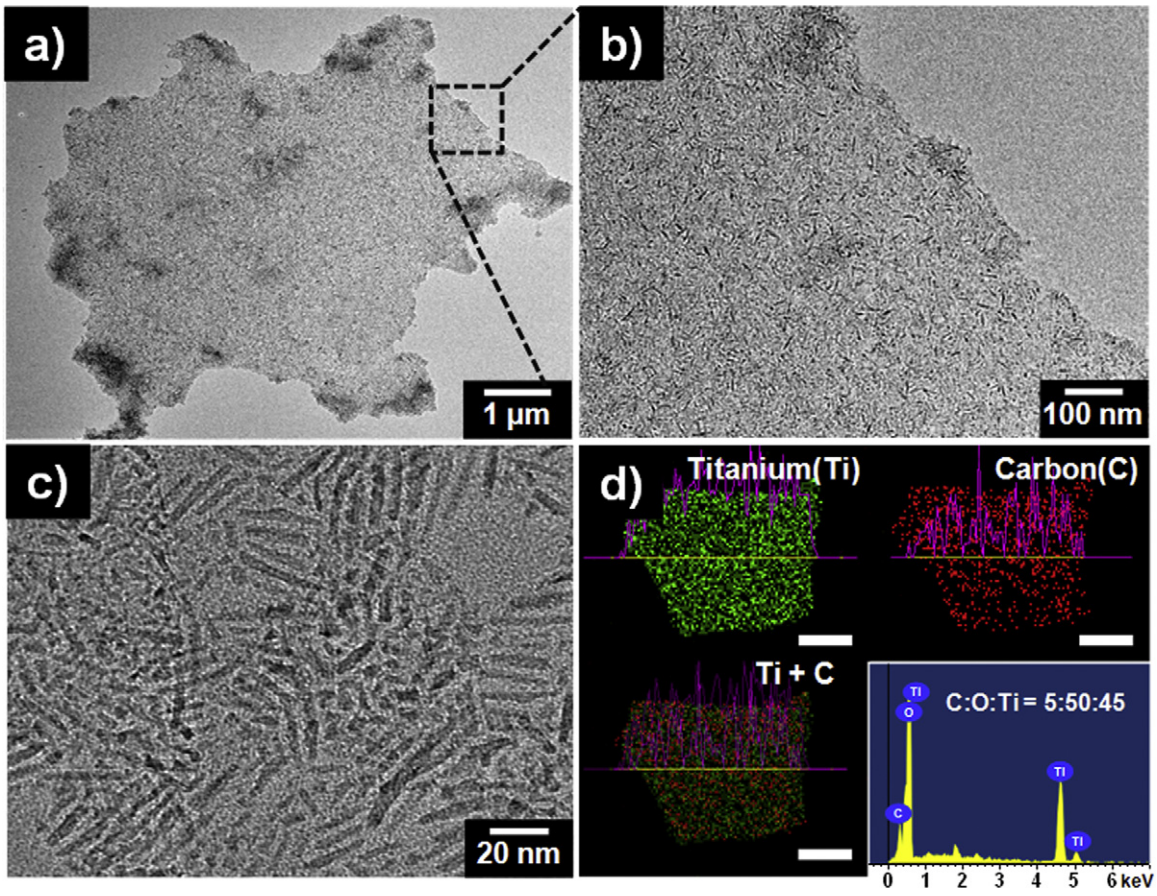

Fig. 1. (a–c) TEM images of as synthesized TNGSs with various magnification. (d) EDS mapping of titanium (Ti), carbon (C), and merged atoms(Ti + C) of TNGSs (scale bar: 2 μm). EDS analysis on selected area of TNGSs.

bandgap by the chemical bonding between TiO_2 NRs and graphene [20]. Accordingly, the introduction of graphene to TiO_2 NRs could expand the light absorption range for the broad visible light-driven photocatalysts.

X-ray photoelectron spectroscopy (XPS) was utilized to investigate the reduction of GO as well as the hybridization of graphene and TiO_2 NRs (Fig. 3a, b). The characteristic peaks of GO in the deconvoluted C1s region appeared at 285.0, 286.1, and 289.2 eV, which were assigned to the C—C, C—O, and C═O functional groups, respectively. In contrast, in the case of the TNGSs, low-intensity oxygen peaks were confirmed, indicating a higher degree of reduction. Moreover, the band at 283.7 eV was assigned to the presence of the Ti—C bond [21,22].

In the case of the Ti2p XPS spectra in Fig. 3b, two bands were located at binding energies of 464.5 and 458.9 eV, which were assigned to $Ti2p_{1/2}$ and $Ti2p_{3/2}$, respectively. The peak deconvolution of the Ti2p spectrum confirmed two low-intensity peaks centered at 465.8 and 460.2 eV, which were assigned to the Ti–C bond [21,22]. On the basis of these results, one may conclude that TiO_2 NRs chemically anchored onto graphene sheets were prepared successfully through the non-hydrolytic sol–gel reaction.

3.2. Photocatalytic activity of TNGSs

To investigate the photocatalytic activity for the as-prepared TNGSs, the photodegradation of MB was carried out under visible light irradiation ($\lambda > 455$ nm) as a model reaction. The reaction kinetics for the photocatalytic degradation of MB was analyzed by the Langmuir–Hinshelwood model. The rate equation for MB degradation can be written as follows [23,24]:

$$r_{MB} = \frac{k_p I_a K_{MB} c_{MB}}{1 + K_{MB} c_{MB}} \quad (1)$$

where K_{MB} is the adsorption equilibrium constant for MB. k_p is the overall rate constant which includes various parameters. I_a is the light intensity which is constant. C_{MB} is the concentration of MB. Considering the competitive adsorption by solvent, intermediates and pollutants, Eq. (1) can be rewritten by k_{ap} as follows:

$$r_{MB} = \frac{k_p I_a K_{MB} c_{MB}}{1 + K_{MB} c_{MB,0}} = k_{ap} c_{MB} \quad (2)$$

where

$$k_{ap} = \frac{k_p I_a K_{MB}}{1 + K_{MB} c_{MB,0}} \quad (3)$$

The integral form of the rate equation is

$$\ln\left(\frac{c_0}{c}\right) = kt \quad (4)$$

The rate constant for MB degradation over P25, TiO_2 NRs, and TNGSs was determined in Fig. S4. It was indicated that the photodegradation of MB over the all the samples roughly follow the pseudo-first-order reaction after 6 h illumination, and the rate constant for MB degradation over P25, TiO_2 NRs, and TNGSs was determined to be 0.8531, 0.2627, and 0.1877 h^{-1}, respectively. It is obvious that TNGSs exhibited the superior photocatalytic activity

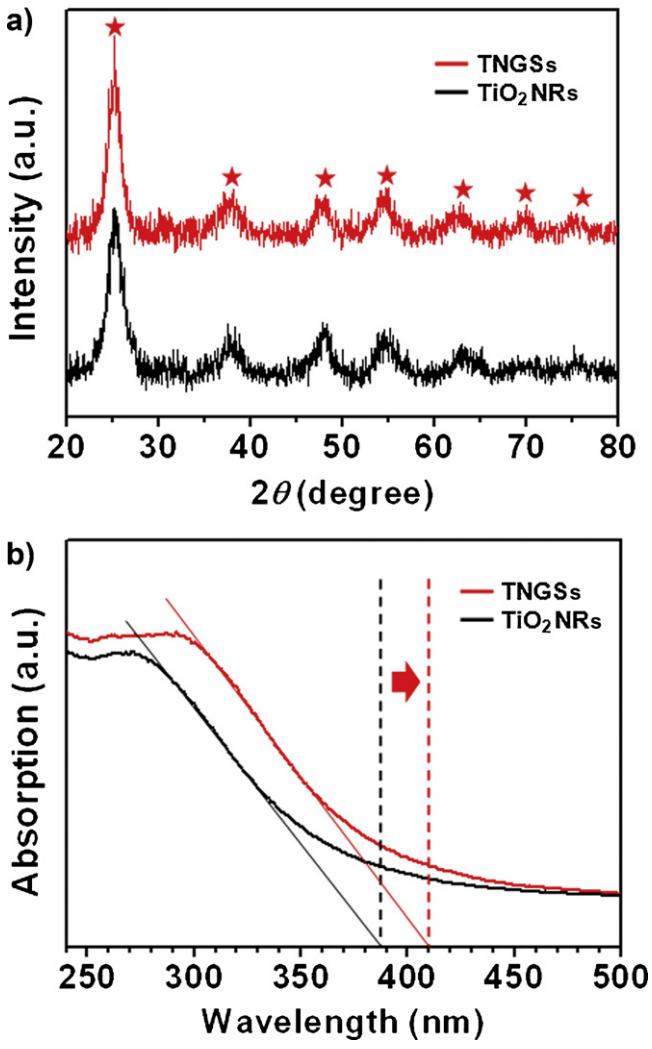

Fig. 2. (a) XRD patterns of TiO_2 NRs (black line) and TNGSs (red line) [star indicates crystalline anatase phase of TiO_2]. (b) UV–vis absorption spectrum patterns of TiO_2 NRs (black line) and TNGSs (red line). The absorption edge of TNGSs indicates red shift ca. 20 nm compared with those of TiO_2 NRs. (For interpretation of the references to color in this figure legend, the reader is referred to the web version of the article.)

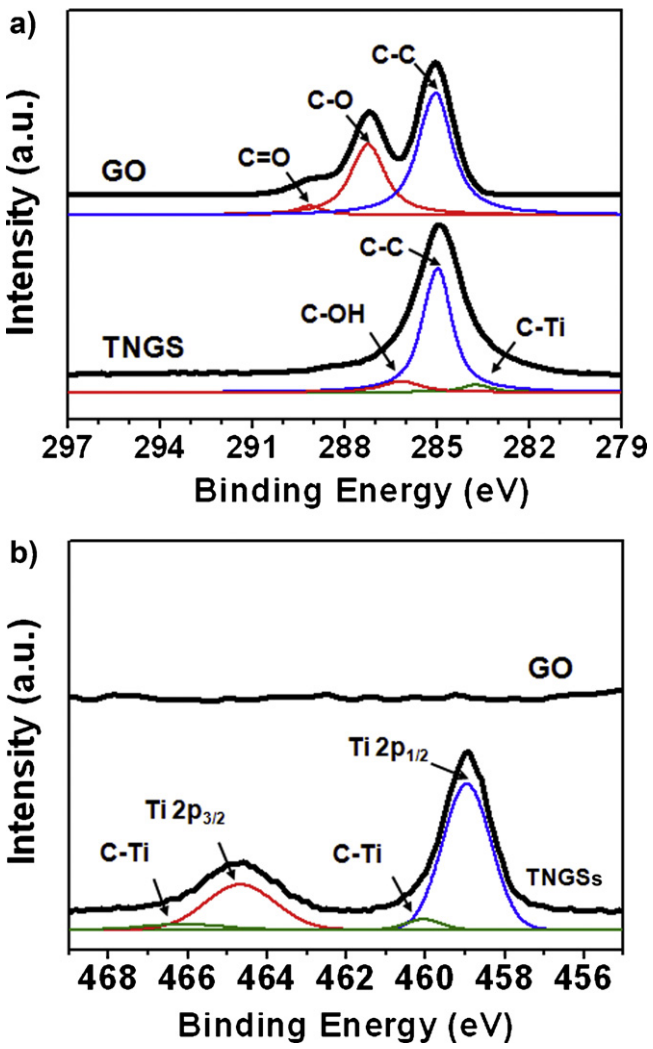

Fig. 3. XPS peak deconvolution of graphene oxide (GO) and TNGSs at (a) the C1s core level and (b) at the Ti2p core level.

for the degradation of MB. Fig. 4 depicts the change in optical density of MB as a function of visible light irradiation time. Importantly, 80% of the primary MB was decomposed by TNGSs (GO 5 wt%) within 2 h. Based on this result, the photocatalytic activity of TNGSs (GO 5 wt%) was about threefold higher than that of the commercial P25. To the best of our knowledge, this result represents the highest photocatalytic activity based on graphene/TiO_2 composite materials [12,14,25]. This high photocatalytic activity can be ascribed to the nanometer-sized TiO_2 NRs and the strong anchoring of TiO_2 NRs on whole graphene layers. The MB degradation rates of TNGSs prepared with various concentration of GO (wt%) are illustrated in Fig. 4a. The MB degradation rate was confirmed to increase significantly up to GO 5 wt% and then decrease gradually with higher concentration of GO (wt%). This tendency of MB degradation rate in concentration of GO (wt%) is consistent with the result of UV light irradiation (see the Supporting Information, Fig. S1). The decrease in photocatalytic activity with high concentration of GO (wt%) can be explained by the increased light absorption into the graphene, as well as the lower relative content of TiO_2 for the generation of radicals [26].

To clarify whether the adsorption or degradation behavior by catalysts was responsible for the degradation of MB, the efficiency of adsorption and photodegradation were determined by measuring the evolution of MB dye concentration (Table 1). The efficiency of MB dye adsorption (E_a) corresponds to the increase of GO weight. This result is consistent with the $\pi-\pi$ stacking interaction between the benzene ring of graphene and MB molecules [27]. Moreover, we confirmed that the efficiency of MB dye photodegradation (E_d) increases significantly (3.2-fold) after the TiO_2 NRs are anchored

Table 1
Efficiencies of adsorption and degradation of MB catalyzed by various samples under visible light.

Sample	C_p[a] (%)	C_0[b] (%)	C_{2h}[c] (%)	E_a[d] (%)	E_d[e] (%)
P25	100	96.4	71.8	3.6	25.5
TiO_2 NRs	100	96.2	61.7	3.8	35.9
TNGSs (GO 1 wt%)	100	81.3	36.3	18.7	51.2
TNGSs (GO 5 wt%)	100	62.1	11.5	37.9	81.5
TNGSs (GO 10 wt%)	100	37.5	25.5	62.5	32.0

[a] Pristine concentration of MB aqueous solution without catalysts (the aqueous solution of MB dyes 3×10^{-5} M).
[b] MB concentration after 2 h reaction in the darkness for the complete adsorption equilibrium. This value is relative MB concentration when C_p is 100% (the weight of catalysts 30 mg).
[c] MB concentration under visible light irradiation for 2 h ($\lambda > 455$ nm).
[d] The efficiency of MB dyes adsorption onto catalysts.
[e] The efficiency of MB dyes photodegradation under visible light irradiation for 2 h.

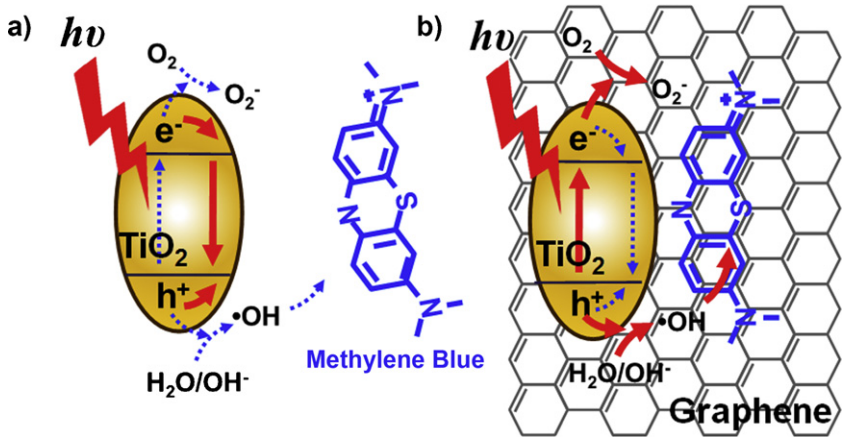

Scheme 1. Schematic illustration of methylene blue photodegradation process with (a) pristine TiO_2 NRs and (b) TNGSs.

on graphene sheets. Taking these results into account, it is concluded that graphene sheets and nanometer-sized TiO_2 in TNGSs (GO 5 wt%) give the highest combined or synergistic contribution to superior photocatalytic activity of MB degradation.

The schematic illustration of the enhanced adsorption and photodecomposition process by TNGSs compared to pristine TiO_2 NRs is summarized in Scheme 1. In the case of TiO_2 NRs, most photogenerated charges are limited in separation and transportation onto the surface of TiO_2 NRs due to the high charge recombination rate. Accordingly, the limited charges can generate "•OH" radicals and "O_2^-" intermediate species by reacting with absorbed H_2O molecules for the photodecomposition of MB. Consequently, in the case of the TNGSs, because the graphene acts as an electron

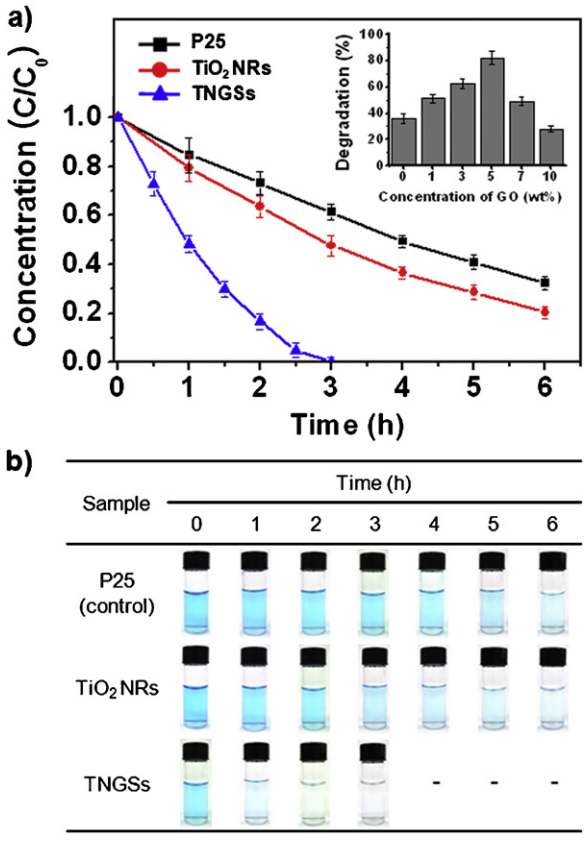

Fig. 4. (a) Photodegradation of MB catalyzed by commercial Degussa P25 (black line), TiO_2 NRs (red line), and TNGSs (GO 5 wt%, blue line) under visible light irradiation ($\lambda > 455$ nm) (inset: the MB photodegradation rate ($(C_0 - C)/C_0 \times 100\%$) catalyzed by the TNGSs prepared with various concentration of GO (wt%) under 2 h visible light illumination). (b) Photographs of the MB solution under visible light irradiation. (For interpretation of the references to color in this figure legend, the reader is referred to the web version of the article.)

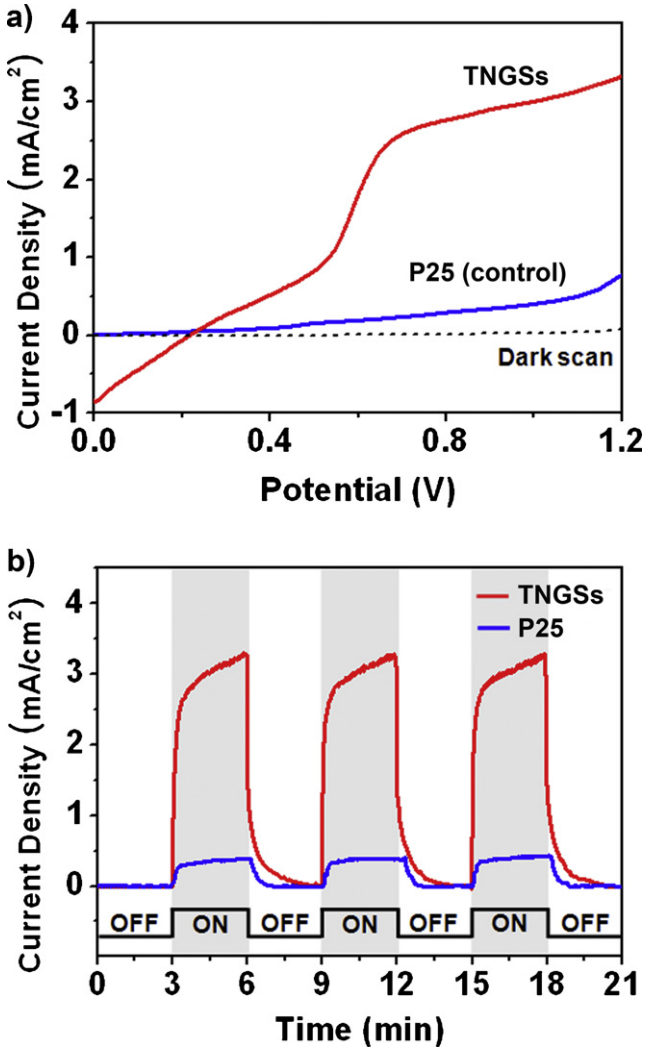

Fig. 5. (a) Linear sweep voltammograms, collected at a scan rate of 10 mV/s from 0 to +1.2 V for P25 (blue) and TNGSs (red). (b) Amperometric *I–t* curves of the P25 and TNGSs at an applied voltage of +1.0 V with 3 min light on/off cycles. (For interpretation of the references to color in this figure legend, the reader is referred to the web version of the article.)

acceptor with high electronic conductivity, photo-generated charges can be separated efficiently and transported to the graphene layer for radical generation [28,29]. Furthermore, the strong π–π stacking interaction between aromatic regions of graphene and MB molecules creates a high affinity and adsorptivity of MB [27]. Therefore, in the photodegradation of MB, the use of TNGSs can show significant improvement over pristine TiO_2 NRs.

3.3. Photoelectrochemistry of TNGSs

It is anticipated that the TNGSs have improved photoelectrochemical properties compared to the pristine TiO_2 because of the synergic incorporation of nanometer-sized TiO_2 NRs and excellent charge transport behavior of graphene sheets [30].

Fig. 5 represents the linear sweep voltammograms and amperometric *I–t* curves of the P25 and TNGSs under UV irradiation condition. When the current density of P25 reached 0.41 mA/cm^2 at 1.0 V, the as-synthesized TNGSs reached 3.0 mA/cm^2 at +1.0 V, which is about 6-fold higher photocurrent density. We believe that the large current enhancement exhibited by TNGSs is due to two factors [31,32]; (i) the large contact surface area of nanometer-sized and well-dispersed TiO_2 NRs and (ii) the integration of high conductive graphene reduce the charge resistance and the charge recombination rate. We also collected amperometric *I–t* curves to study the photoresponse of P25 and TNGSs. With three light on/off cycles, distinct changes of photocurrent by P25 and TNGSs have been showed in Fig. 5b. Furthermore, large enhancement of photocurrent with light irradiation was shown, which is well correspond to the results of the linear sweep voltammograms.

4. Conclusions

In conclusion, a facile method for the fabrication of TiO_2 nanocrystals/graphene composites was demonstrated using a non-hydrolytic sol–gel reaction. The as-prepared TNGSs indicated that well-dispersed TiO_2 nanorods (diameter 4 nm × length 25 nm) were anchored on the graphene sheets. Furthermore, the population of TiO_2 on the graphene sheets were controlled by adjusting the concentration of GO. Interestingly, the incorporation of graphene with TiO_2 expanded the light absorption, in addition, enhanced the photocatalytic decomposition of methylene blue molecules. From the photoelectrochemical analysis, the primary role of graphene in TNGSs was confirmed as an electron conductor, enhancing the photocurrent density. The developed methodology may provide a convenient way for the incorporation between graphene and various metal oxides.

Acknowledgement

This work was supported by WCU (World Class University) program through the National Research Foundation of Korea funded by the Ministry of Education, Science and Technology (R31-10013).

Appendix A. Supplementary data

Supplementary data associated with this article can be found, in the online version, at doi:10.1016/j.jhazmat.2011.12.033.

References

[1] H. Kong, J. Song, J. Jang, Photocatalytic antibacterial capabilities of TiO_2-biocidal polymer nanocomposites synthesized by a surface-initiated photopolymerization, Environ. Sci. Technol. 44 (2010) 5672–5676.
[2] Z.R. Tian, J.A. Voigt, J. Liu, B. McKenzie, M.J. McDermott, M.A. Rodriguez, H. Konishi, H. Xu, Complex and oriented ZnO nanostructures, Nat. Mater. 2 (2003) 821–826.
[3] C. Kim, M. Choi, J. Jang, Nitrogen-doped SiO_2/TiO_2 core/shell nanoparticles as highly efficient visible light photocatalyst, Catal. Commun. 11 (2010) 378–382.
[4] M. Miyauchi, A. Nakajima, T. Watanabe, K. Hashimoto, Photocatalysis and photoinduced hydrophilicity of various metal oxide thin films, Chem. Mater. 14 (2002) 2812–2816.
[5] S.H. Hwang, C. Kim, J. Jang, SnO_2 nanoparticle embedded TiO_2 nanofibers—highly efficient photocatalyst for the degradation of rhodamine B, Catal. Commun. 12 (2011) 1037–1041.
[6] A. Fujishima, K. Honda, Electrochemical photolysis of water at a semiconductor electrode, Nature 238 (1972) 37–38.
[7] R. Leary, A. Westwood, Carbonaceous nanomaterials for the enhancement of TiO_2 photocatalysis, Carbon 49 (2011) 741–772.
[8] M. Grätzel, Solar energy conversion by dye-sensitized photovoltaic cells, Inorg. Chem. 44 (2005) 6841–6851.
[9] K. Vinodgopal, D.E. Wynkoop, P.V. Kamat, Environmental photochemistry on semiconductor surfaces: photosensitized degradation of a textile azo dye, Acid Orange 7, on TiO_2 particles using visible light, Environ. Sci. Technol. 30 (1996) 1660–1666.
[10] A.K. Geim, K.S. Novoselov, The rise of graphene, Nat. Mater. 6 (2007) 183–191.
[11] K.-Y. Shin, J.-Y. Hong, J. Jang, Micropatterning of graphene sheets by inkjet printing and its wideband dipole-antenna application, Adv. Mater. 23 (2011) 2113–2118.
[12] K. Zhou, Y. Zhu, X. Yang, X. Jiang, C. Li, Preparation of graphene–TiO_2 composites with enhanced photocatalytic activity, New J. Chem. 35 (2011) 353.
[13] D. Wang, D. Choi, J. Li, Z. Yang, Z. Nie, R. Kou, D. Hu, C. Wang, L.V. Saraf, J. Zhang, I.A. Aksay, J. Liu, Self-assembled TiO_2-graphene hybrid nanostructures for enhanced Li-ion insertion, ACS Nano 3 (2009) 907–914.
[14] H. Zhang, X. Lv, Y. Li, Y. Wang, J. Li, P25-graphene composite as a high performance photocatalyst, ACS Nano 4 (2010) 380–386.
[15] G. Williams, B. Seger, P.V. Kamt, TiO_2-graphene nanocomposites. UV-assisted photocatalytic reduction of graphene oxide, ACS Nano 2 (2008) 1487–1491.
[16] T.N. Lambert, C.A. Chavez, B. Hernandez-Sanchez, P. Lu, N.S. Bell, A. Ambrosini, T. Friedman, T.J. Boyle, D.R. Wheeler, D.L. Huber, Synthesis and characterization of titania-graphene nanocomposites, J. Phys. Chem. C 113 (2009) 19812–19823.
[17] W.S. Hummers Jr., R.E. Offeman, Preparation of graphitic oxide, J. Am. Chem. Soc. 6 (1958) 1339.
[18] B. Koo, J. Park, Y. Kim, S.H. Choi, Y.E. Sung, T. Hyeon, Simultaneous phase- and size-controlled synthesis of TiO_2 nanorods via non-hydrolytic sol–gel reaction of syringe pump delivered precursors, J. Phys. Chem. B 110 (2006) 24318–24323.
[19] H. Yoon, J. Jang, Conducting-polymer nanomaterials for high-performance sensor applications: issues and challenges, Adv. Funct. Mater. 19 (2009) 1567–1576.
[20] S. Sakthivel, H. Kisch, Daylight photocatalysis by carbon-modified titanium dioxide, Angew. Chem. Int. Ed. 42 (2003) 4908–4911.
[21] O. Akhavan, E. Ghaderi, Photocatalytic reduction of graphene oxide nanosheets on TiO_2 thin film for photoinactivation of bacteria in solar light irradiation, J. Phys. Chem. C 47 (2009) 20214–20220.
[22] Y. Huang, W. Ho, S. Lee, L. Zhang, G. Li, J.C. Yu, Effect of carbon doping on the mesoporous structure of nanocrystalline titanium dioxide and its solar-light-driven photocatalytic degradation of NO_x, Langmuir 24 (2008) 3510–3516.
[23] F. Jiang, Z. Zheng, Z. Xu, S. Zheng, Preparation and characterization of SiO_2-pillared $H_2Ti_4O_9$ and its photocatalytic activity for methylene blue degradation, J. Hazard. Mater. 164 (2009) 1250–1256.
[24] J.K. Zhou, L. Lv, J. Yu, H.L. Li, P. Guo, H. Sun, X.S. Zhao, Synthesis of self-organized polycrystalline F-doped TiO_2 hollow microspheres and their photocatalytic activity under visible light, J. Phys. Chem. C 112 (2008) 5316–5321.
[25] J. Liu, H. Bai, Y. Wang, Z. Liu, X. Zhang, D.D. Sun, Self-assembling TiO_2 nanorods on large graphene oxide sheets at a two-phase interface and their anti-recombination in photocatalytic applications, Adv. Funct. Mater. 20 (2010) 4175–4181.
[26] Y.B. Tang, C.S. Lee, J. Xu, Z.T. Liu, Z.H. Chen, Z. He, Y.L. Cao, G. Yuan, H. Song, L. Chen, L. Luo, H.M. Cheng, W.J. Zhang, I. Bello, S.T. Lee, Incorporation of graphenes in nanostructured TiO_2 films via molecular grafting for dye-sensitized solar cell application, ACS Nano 4 (2010) 3482–3488.
[27] Z. Liu, J.T. Robinson, X. Sun, H. Dai, PEGylated nanographene oxide for delivery of water-insoluble cancer drugs, J. Am. Chem. Soc. 130 (2008) 10876–10877.
[28] X. Wang, L. Zhi, K. Müllen, Transparent, conductive graphene electrodes for dye-sensitized solar cells, Nano Lett. 8 (2008) 323–327.
[29] Q. Liu, Z. Liu, X. Zhang, L. Yang, N. Zhang, G. Pan, S. Yin, Y. Chen, J. Wei, Polymer photovoltaic cells based on solution-processable graphene and P3HT, Adv. Funct. Mater. 19 (2009) 894–904.
[30] N. Yang, J. Zhai, D. Wang, Y. Chen, L. Jiang, Two-dimensional graphene bridges enhanced photoinduced charge transport in dye-sensitized solar cells, ACS Nano 4 (2010) 887–894.
[31] H. Fei, Y. Yang, D.L. Rogow, X. Fan, S.R.J. Oliver, Polymer-templated nanospider TiO_2 thin films for efficient photoelectrochemical water splitting, ACS Appl. Mater. Interfaces 2 (2010) 974–979.
[32] N.J. Bell, Y.H. Ng, A. Du, H. Coster, S.C. Smith, R. Amal, Understanding the enhancement in photoelectrochemical properties of photocatalytically prepared TiO_2-reduced graphene oxide composite, J. Phys. Chem. C 115 (2011) 6004–6009.